APPENDIX G

REFERENCES

Rudnicki, J.W. 1999. Alteration of regional stress by reservoirs and other inhomogeneities: Stabilizing or destabilizing? Pp. 1629-1637 in *Proceedings of the Ninth International Congress on Rock Mechanics*, edited by G. Vouille and P. Berest. London: Taylor & Francis.

Rudnicki, J.W. 2002. Eshelby transformations, pore pressure and fluid mass changes, and subsidence. Pp. 307-312 in *Poromechanics II, Proceedings of the Second Biot Conference on Poromechanics*, edited by J.-L. Auriault et al. Leiden: A.A. Balkema.

Terzaghi, K. 1940. *Theoretical Soil Mechanics*. New York: Wiley.

APPENDIX H

Pore Pressure Induced by Fluid Injection

The dependence of the induced pore pressure on the operation parameters (injection rate, volume of fluid injected), on position and time, and on the hydraulic properties of the reservoir is illustrated in this appendix by considering the simple example of fluid injection in a disk-shaped reservoir. The analysis shows that different parameters control the pore pressure at the beginning of the injection operation and once enough fluid has been injected in the reservoir (see also Nicholson and Wesson, 1990).

The pore pressure induced by injection of fluid, $\Delta\rho$, is to a good approximation governed by the diffusion equation

$$c\nabla^2\Delta\rho = \partial\Delta\rho/\partial t + \text{source}$$

where c denotes the hydraulic diffusivity equal to $c = k/\mu S$. In the above, k is the intrinsic permeability of the rock (generally expressed in Darcy), μ is the fluid viscosity, and S is the storage coefficient, a function of the compressibility of both the fluid and the porous rock. The diffusion equation imposes a certain structure on the link between the magnitude of the induced pore pressure $\Delta\rho$, the injected fluid volume V, and the rate of injection Q_o.

As an example, we consider the injection of fluid at a constant volumetric rate Q_o, at the center of a disk-shaped reservoir of thickness H and radius R. It is assumed that the reservoir is thin (i.e., $H/R \ll 1$), and also that the pore pressure is uniform over the thickness of the layer, which implies, depending on the manner the fluid is injected, that some time has elapsed since the beginning of the operation.

At early time (to be defined more precisely later), the pore pressure perturbation induced by injection of fluid has not reached the boundary of the reservoir. The induced pore pressure field is then given by the source solution for an infinite domain, a solution of the form (Wang, 2000)

$$\Delta\rho(r,t) = \rho_* F(r/\sqrt{[ct]}) \qquad (1)$$

where r is the radial distance from the injection well, t is time, and F is a known function. The quantity where ρ_* is a characteristic pressure (i.e., a yardstick for measuring the induced pressure) given by

$$\rho_* = \mu Q_o/kH$$

APPENDIX H

Once the time elapsed since injection started becomes larger than a fraction, say 0.1, of the characteristic time $t_* = R^2/c$, then the evolution of the induced pore pressure becomes influenced by the finiteness of the reservoir. Formally, the pore pressure solution can then be expressed as

$$\Delta\rho(r,t) = \rho_* P(r/R,\ t/t_*) \tag{2}$$

The function $P(\rho,t)$ can be determined semianalytically. If the elapsed time t is expressed as the ratio of the injected volume V to the rate of injection Q_o (i.e., $t=V/Q_o$), then solution (2) can be written as

$$\Delta\rho(r,V) = \rho_* P(r/R\ ,V/V_*) \tag{3}$$

where $V_* = (Q_o R^2)/c$ is a characteristic fluid volume. The above expression suggests that the relationship between the induced pore pressure $\Delta\rho$, the injected volume V, and the injection rate Q_o is not straightforward. However, Equation (3) shows important trends; for example, a decrease of the permeability causes an increase of the characteristic pressure, or an increase of the storage coefficient causes a decrease of the pore pressure, all other parameters kept constant.

At small time $t \ll t_*$, the dimensionless pressure $P = \Delta\rho/\rho_*$ reduces to the unbounded domain solution F, while at large time $t \gg t_*$, the pressure tends to become uniform and the pore pressure is simply given by

$$\rho \cong V/(\pi R^2 HS) \tag{4}$$

as the function $P(\rho,t)$ behaves for large t as $P \cong t/\pi$. Thus, at large time, the pore pressure is simply proportional to the volume of injected fluid (Figure H.1). Equation (4) actually indicates that the large-time pore pressure is simply the ratio of the injected volume over the reservoir volume, divided by the storage coefficient.

The previous material provides some information about the link between pore pressure, injected volume, and injected rate for the particular case of an injector centered in a disk-shaped reservoir. These ideas can be generalized to more realistic cases. For example, for an arbitrarily shaped reservoir with n wells, each injecting at a rate Q_o, the general expression for the induced pore pressure can be written as

$$\Delta\rho(x,t) = \rho_* \varsigma\{x/L,\ t/t_*;\ n,\ (x_i,\ i=1,\ n),\ \textit{reservoir shape}\}$$

where the characteristic pressure and time are given by

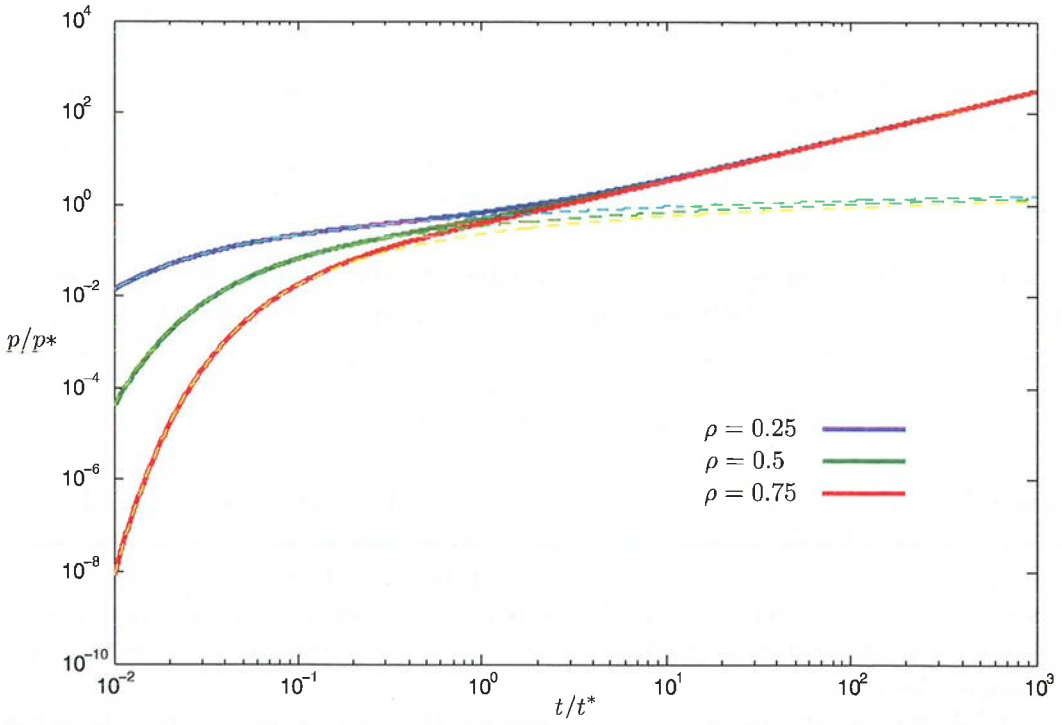

FIGURE H.1 Injection of fluid at a constant rate at the center of a disk-shaped reservoir. Plot of the dimensionless pore pressure $\Delta p/p_*$ with respect to the dimensionless time $t = t/t_*$ (equal to V/V_*) for three values of the dimensionless radius $Q = r/R$. This plot indicates that the pressure response is similar to the response of an unbounded reservoir as long as $t \leq 0.2$ and that the pressure is approximately uniform and proportional to the volume of fluid injected when $t \geq 10$. The dashed-line curves correspond to the solution ***F*** for an unbounded reservoir.

$$p_* = \mu Q_o/kL, \; t_* = L^2/c$$

with L denoting a relevant length scale of the reservoir. Also x refers to the position of the field point, and x_i to the position of the source i. At large time, the induced pore pressure is approximately given by

$$p \cong V/(SV_{reservoir})$$

where V is the total volume of fluid injected ($V = nQ_o t$) and $V_{reservoir}$ is the volume of the reservoir.

APPENDIX H

REFERENCES

Nicholson, C., and R.L. Wesson. 1990. Earthquake Hazard Associated with Deep Well Injection: A Report to the U.S. Environmental Protection Agency. U.S. Geological Survey Bulletin 1951, 74 pp.

Wang, H.F. 2000. *Theory of Linear Poroelasticity with Applications to Geomechanics and Hydrogeology*. Princeton, NJ: Princeton University Press.

APPENDIX I

Hydraulic Fracture Microseismic Monitoring

During a hydraulic fracture operation, very small earthquakes (**M** -4 to 0) (microseismic events) are induced from the high-pressure injection of fluids into the subsurface. These "microearthquakes" are thought to be caused by the increase in pore pressure leaking off into rock surrounding the hydraulic fracture. The increased pore pressure causes small natural fractures in the formation to slip, causing microearthquakes. These microearthquakes are thousands of times smaller than a typical earthquake that can be felt by humans. Recording and location analysis of microseismicity requires specialized seismic sensing equipment and processing algorithms. The location and size of the microseismicity are used by oil and gas operators to help determine the geometry of hydraulic fractures in the formation. Microseismic mapping is a very useful tool in planning fieldwide well development programs, such as horizontal well direction and the spacing between wells, as well as aiding the design of hydraulic fracturing procedures, such as injection rate and fluid volume. Microseismic data are acquired with either an array of seismic instruments (geophones or accelerometers) in one or multiple wellbores, or with a large number (100 to more than 1,000) of geophones near or on the surface (Figure I.1). Specialized data processing techniques are used to precisely locate the microseismic events in time and space and to compute source parameters such as seismic moment, magnitude, and moment tensors, if the data are adequate.

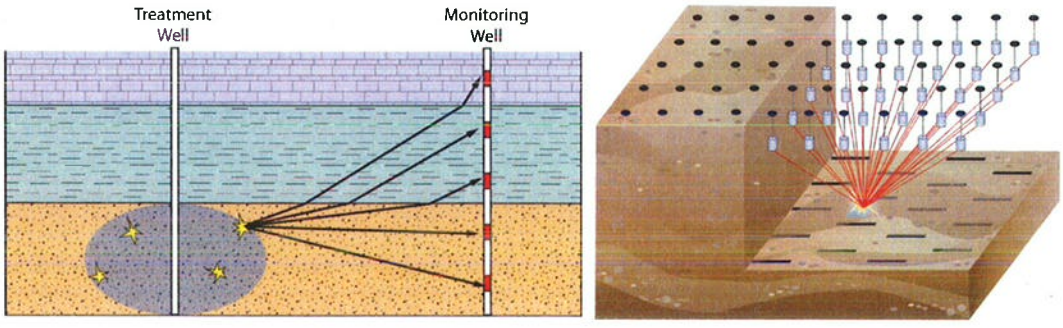

FIGURE I.1 Diagram demonstrating microseismic monitoring of a hydraulic fracture. The hydraulic fracture induces microearthquakes that are recorded with seismometers in a nearby well bore (left) or a large number of seismometer instruments placed on or near the surface (right). SOURCE: Left, courtesy MEQ Geo Inc.; right, courtesy of MicroSeismic, Inc.

APPENDIX I

The hydraulic fractures typically propagate parallel to the maximum stress direction in the reservoir. In areas of low stress differences, the hydraulic fracture pattern can be quite complex, as there is no preferential direction for the fracture to grow, in contrast with areas of high stresses, where the hydraulic fracture grows parallel to the maximum stress direction. Figure I.2 shows two examples of microseismic mapping results following hydraulic fracturing procedures in Texas: an example from the Barnett shale gas horizontal well showing a complex fracture geometry (right), and the other from tight gas sands in a vertical well in the Cotton Valley formation, which shows a simple fracture geometry (left).

Microseismic mapping with borehole or surface sensors can be used to distinguish between reactivated natural faulting and hydraulic fracture events, through **b** value analysis (see Appendix D). Hydraulic fracture wells are often drilled to avoid large natural faults distinguished from three-dimensional surface seismic images, as faults can "steal" fracturing fluid and divert fluids away from the formation targeted for hydraulic fracturing. An example of this issue was discussed by Wessels et al. (2011), where a through-going fault was reactivated during hydraulic fracturing (Figure I.3).

REFERENCES

Maxwell, S.C., J. Rutledge, R. Jones, and M. Fehler. 2010. Petroleum reservoir characterization using downhole microseismic monitoring. *Geophysics* 75(5):75A129-75A137.

Warpinski, N.R., R.C. Kramm, J.R. Heinze, and C.K. Waltman. 2005. Comparison of single- and dual-array microseismic mapping techniques in the Barnett Shale. Presented at the Society of Petroleum Engineers Annual Technical Conference and Exhibition, Dallas, TX, October 9-12.

Wessels, S.A., A. De La Pena, M. Kratz, S. Williams-Stroud, and T. Jbeili. 2011. Identifying faults and fractures in unconventional reservoirs through microseismic monitoring. *First Break* 29(7):99-104.

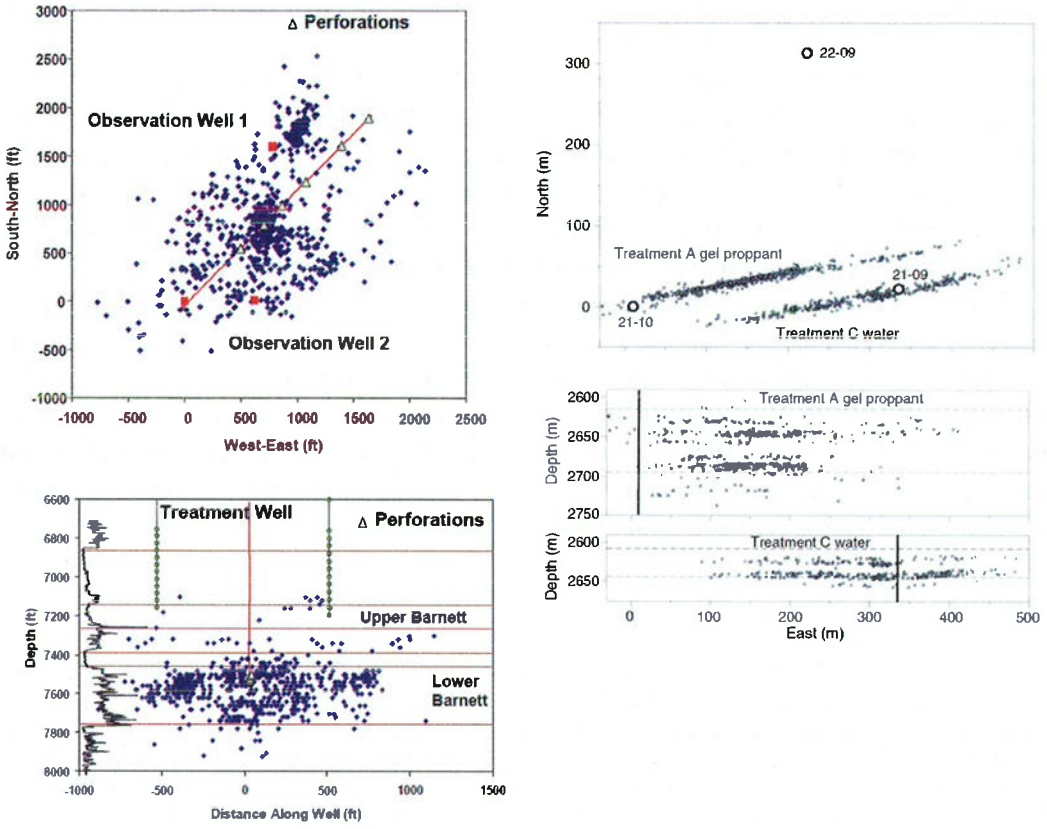

FIGURE I.2 Examples of microseismic borehole monitoring results following hydraulic fracturing procedure. (a) On the left is a map (top) and cross section (bottom) view in the Barnett Shale after a multistage hydraulic fracture treatment in a horizontal well (red line, triangles indicate perforation in wellbore where fluid is injected); the small blue dots show the location of microseismic events mapped from two borehole observation wells shown by red squares; seismic instruments are indicated by green circles. (b) On the right is a map (top) and two cross-section (bottom) views of two vertical hydraulic fractured wells (white circles) drilled in the tight gas sands of the Cotton Valley Formation. The small gray dots show microseismic locations during a gel-based and water-based hydraulic fracturing fluid injection. SOURCE: Left, Warpinski et al. (2005); right, Maxwell et al. (2010).

APPENDIX I

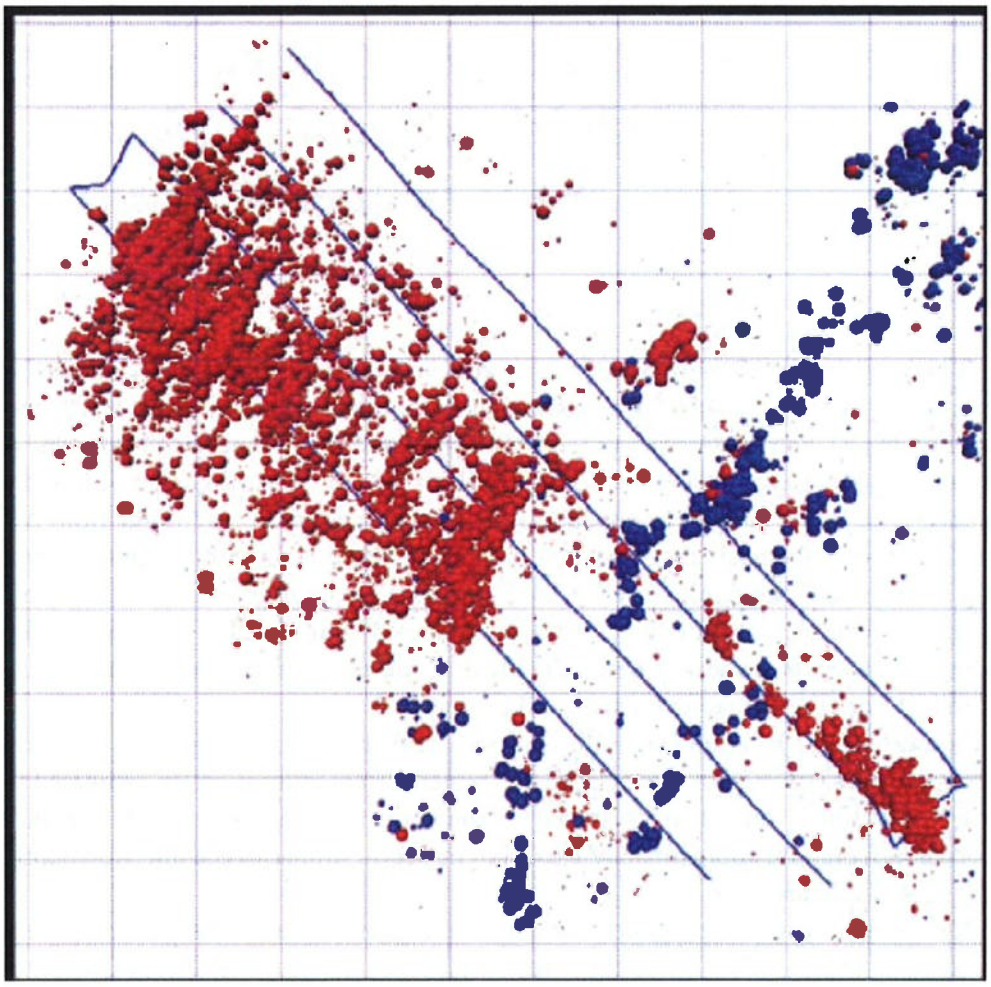

FIGURE I.3 Map view of hydraulic fracture microseismic events during a four-well stimulation (dark blue lines on the map) in the Barnett Shale. Red events are interpreted to be associated with hydraulic fracturing; blue dots indicate microseismicity associated with the reactivation of a strike-slip fault. See Wessels et al. (2011) for details. Some hydraulic fracture stages were not mapped. SOURCE: Wessels et al. (2011).

APPENDIX J

Hydraulic Fracturing in Eola Field, Garvin County, Oklahoma, and Potential Link to Induced Seismicity

A hydraulic fracture treatment in January 2011 in Eola field, Oklahoma, coincided with a series of earthquakes. Eola field is located in central Oklahoma, southwest of Oklahoma City (Figure J.1). Felt seismicity was reported on the evening of January 18 from one resident near Elmore City, Oklahoma. Further analysis showed 50 earthquakes occurred that evening, 43 of which were large enough to be located, ranging in magnitude from **M** 1.0 to **M** 2.8. The earthquakes are coincident in location and timing with a hydraulic fracture in the Eola field, Picket Unit B well 4-18. The events all occurred within 24 hours of the first activity. The deepest hydraulic fracture in the Picket Unit B well 4-18 occurred 7 hours before the first earthquake was detected. Most of the events appear to be about 3.5 km (2.2 miles) from the hydraulic fracture well (Figure J.2).

Accurate event locations were difficult to establish; the closest seismic station was 35 km (22 miles) away from the locus of the events. Errors in location are estimated to be 100-500 m (~100 to more than 500 yards) in ground distance and twice that for depth. The hypocenter depths are approximately 1 to 5 km in depth, similar to the injection depth for the 4-18 well (Figure J.3).

Other cases of suspected induced activity in Oklahoma have been reported in the past. For example, in June 1978, 70 earthquakes occurred in 6.2 hours in Garvin County after a hydraulic fracture treatment. In May 1979, a well was stimulated over a 4-day period, where three different formations were hydraulically fractured over at depths of 3.7, 3.4, and 3.0 km (2.2 to 1.8 miles). The first and deepest hydraulic fracture stage was followed by 50 earthquakes over the next 4 hours. The second stage was followed immediately by 40 earthquakes in 2 hours; no activity was associated with the third and shallowest hydraulic fracture (Nicholson and Wesson, 1990). The largest event in the sequence was **M** 1.9. Just two of the earthquakes were felt. The activity was 1 km (0.6 miles) away from the Wilson seismic station in Oklahoma.

South central Oklahoma has experienced historical seismicity (Figure J.4) and has been the most seismically active part of the state since 1977. A series of Earthscope Transportable Array stations were located near the events by coincidence; without these stations, a majority of the earthquakes could not be located.

APPENDIX J

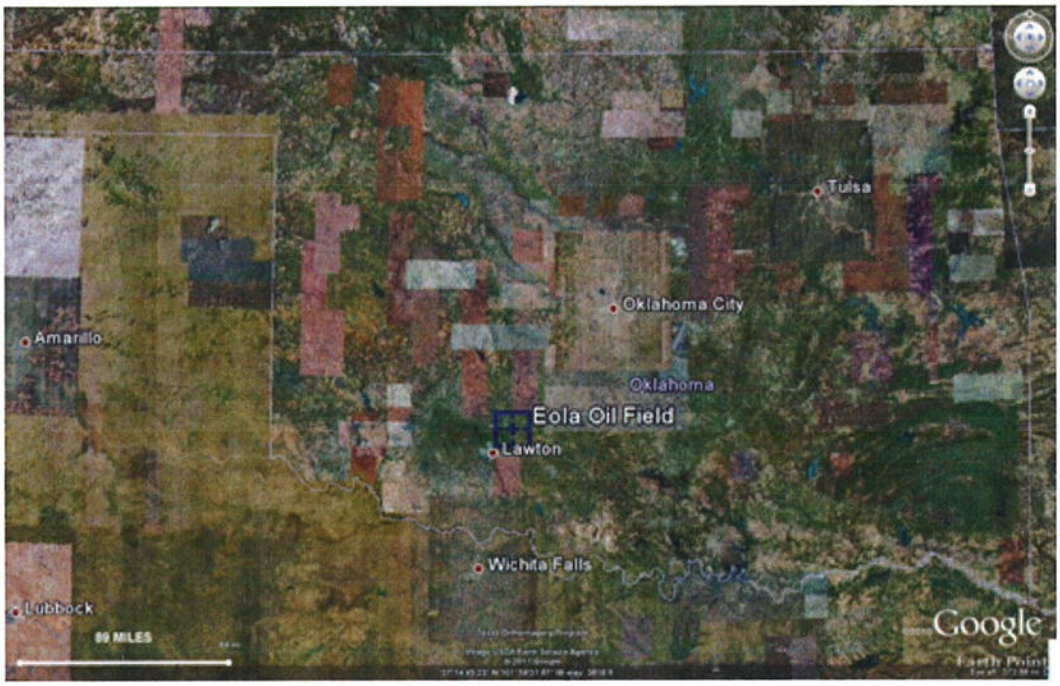

FIGURE J.1 Google Earth image showing the state of Oklahoma and the location of the Eola oil field. SOURCE: Google Earth.

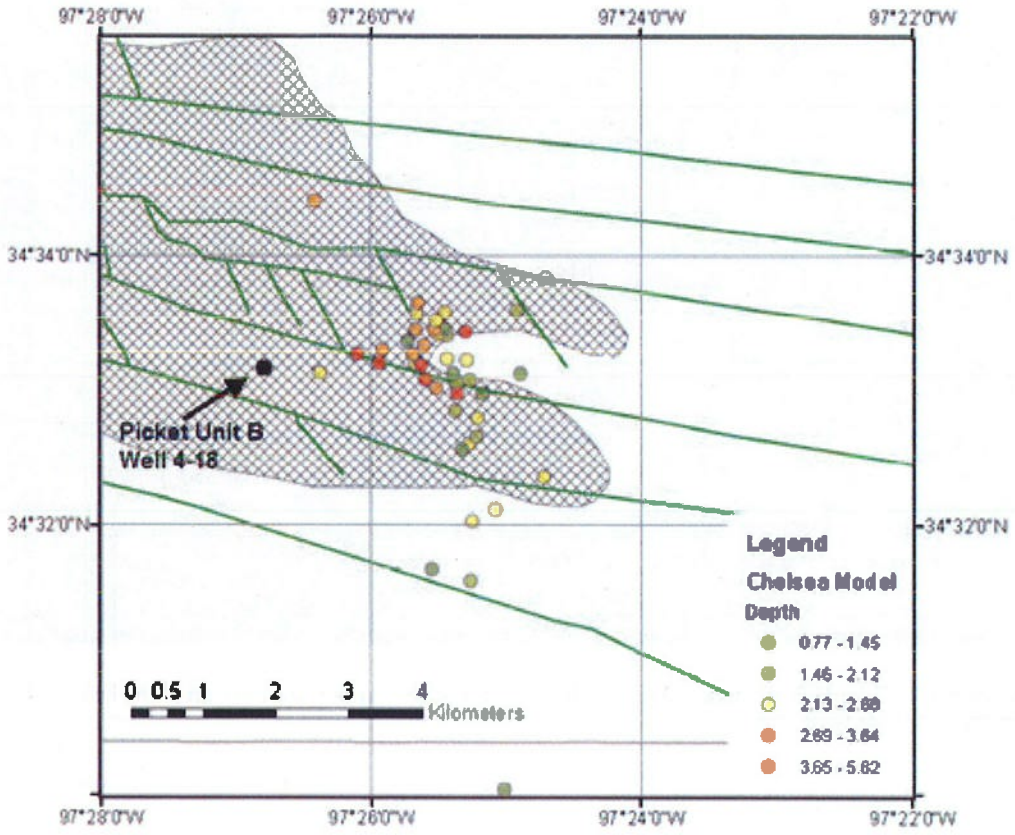

FIGURE J.2 Map of earthquake locations, the Picket Unit B Well 4-18. The Eola field is outlined by the gray hashed area. Faults mapped by Harlton (1964) are marked by green lines. SOURCE: Holland (2011).

APPENDIX J

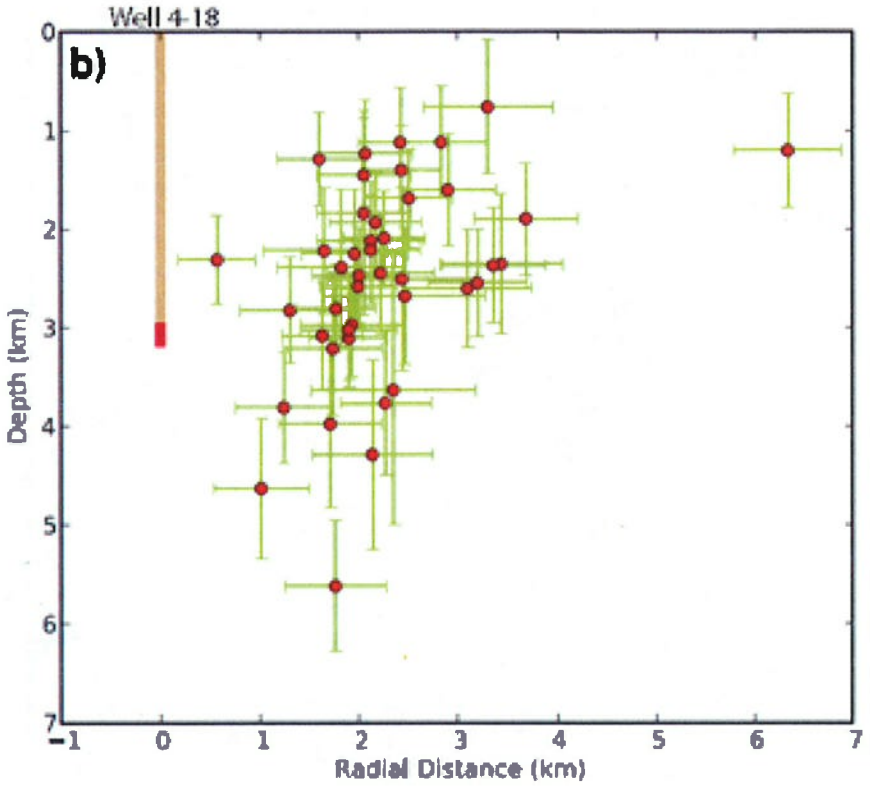

FIGURE J.3 Depth distribution of hypocenters and uncertainty estimates with respect to the fracture well 4.18. SOURCE: Holland (2011).

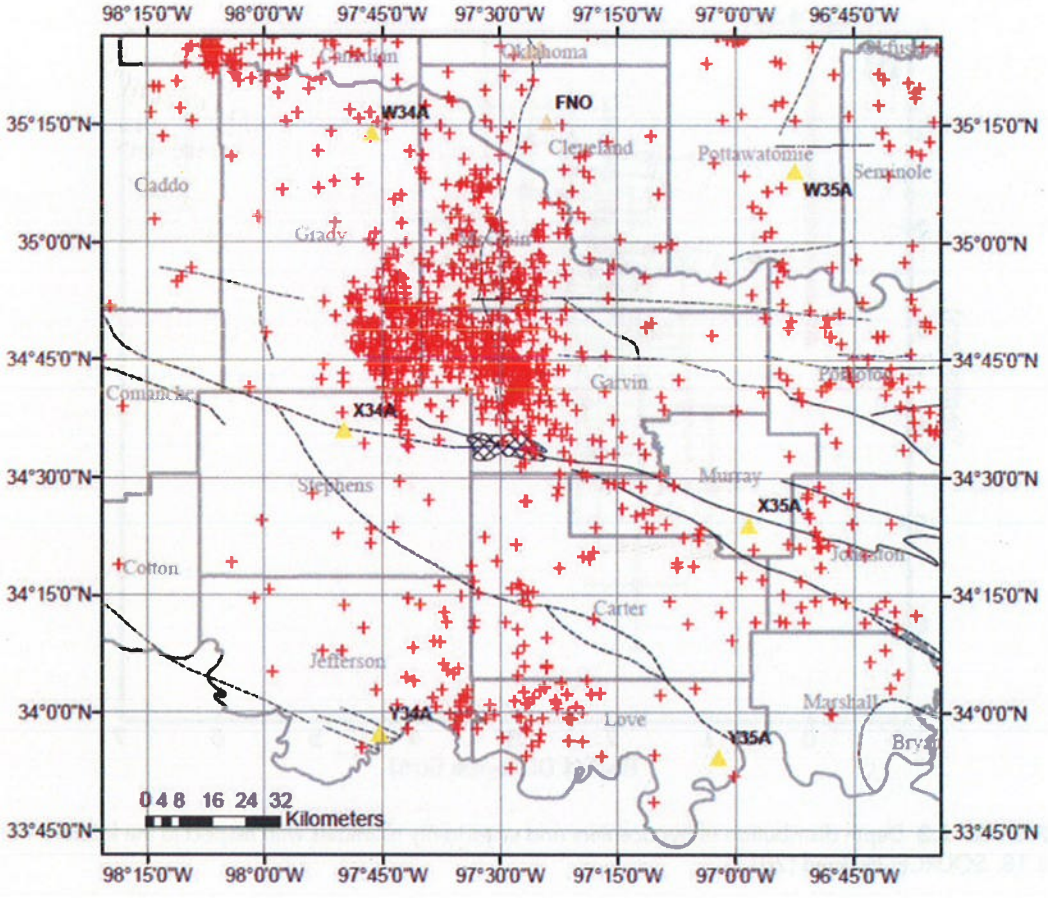

FIGURE J.4 Map of historical seismicity from the Oklahoma Geological Survey catalog. Earthquakes from 1897 to 2010 are shown by red crosses. SOURCE: Holland (2011).

APPENDIX J

REFERENCES

Harlton, B.H. 1964. Tectonic framework of Eola and Southeast Hoover oil fields and West Timbered Hills area, Garvin and Murray counties, Oklahoma. *Bulletin of the American Association of Petroleum Geologists* 48(9):1555-1567.

Holland, A. 2011. Examination of possibly induced seismicity from hydraulic fracturing in the Eola Field, Garvin County, Oklahoma. Oklahoma Geological Survey Open-File Report OF1-2011. Available at www.ogs.ou.edu/pubsscanned/openfile/OF1_2011.pdf. Accessed April 2012.

Nicholson, C., and R.L. Wesson. 1990. Earthquake Hazard Associated with Deep Well Injection—A Report to the U.S. Environmental Protection Agency. U.S. Geological Survey Bulletin 1951, 74 pp.

APPENDIX K

Paradox Valley Unit Saltwater Injection Project

The Colorado River Basin Salinity Control Project is located in Montrose County, on the western border of Colorado. The project diverts naturally occurring seepage of salt brine that would normally flow into the Delores River (and then into the Colorado River) and injects the brine underground. The project is operated by the U.S. Department of the Interior, Bureau of Reclamation. Due to concerns of induced seismicity, seismic data for this project have been continuously recorded and analyzed since the project began in 1996 in order to understand and mitigate the effects of any induced seismic events.

The Paradox Valley Unit (PVU) is a group of wells that are part of this project. The brine is produced from nine extraction wells before it can flow into the Delores River. The brine is then injected into one disposal well. The well is located near the town of Bedrock, Colorado, approximately 1 mile southwest of the extraction wells. The well injects the brine into a limestone formation at a depth of approximately 14,100 to 15,750 feet. The project began in July 1996 with an initial injection rate of 345 gallons per minute at a pressure of 4,900 psi. Current injection rates are approximately 230 gallons per minutes at a pressure of 5,300 psi.

The possibility of induced seismicity was addressed during the planning stages of the PVU injection program because the Paradox Valley Unit injection program was comparable to both the injection programs at the Rocky Mountain Arsenal northeast of Denver and the water injection program for improved oil recovery at Rangely, Colorado. Eight years before injection was begun at the PVU site, the Bureau of Reclamation commissioned a seismic monitoring network to measure the seismic activity in the Paradox Valley region. The original network consisted of 10 seismic monitoring stations. The system was upgraded to 16 stations after the injection began in 1996 and currently totals 20 stations.

Earthquakes were recorded almost immediately after the beginning of injection in July 1996 with the first seismic event measured in November 1996. Minor earthquakes continued through mid-1999, and two magnitude 3.5 events occurred in June and July 1999. In response to the higher-magnitude earthquakes, the Bureau of Reclamation initiated a program to cease injection for 20 days every 6 months. Prior to these events they had noted the rate of seismicity had decreased during the shutdowns following unscheduled maintenance. The Bureau of Reclamation hoped stopping injection twice yearly would allow time for the injection fluid to diffuse from the pressurized fractures into the rock matrix.

After a magnitude 4.3 earthquake occurred in May 2000, PVU stopped injection for 28 days to allow evaluation of the injection program and its relationship to induced seismic

events. After analysis the injection rate was decreased by one-third from 345 gallons per minute to 230 gallons per minute. The program of ceasing injection for 20 days twice per year was also continued from June 2000 to January 2002 as were the lower injection rates.

In January 2002 the injection fluid was changed to 100 percent brine water from a mixture of 70 percent brine with 30 percent freshwater, which was the injection mixture from the start of the project. This heavier fluid increased the hydrostatic pressure measured at the bottom of the injection well but no difference in the rate of induced seismicity resulted from this change.

After monitoring injection into the Paradox Valley Unit injection well for almost 15 years, the Bureau of Reclamation has recorded over 4,600 induced seismic events. The largest seismic event occurred on May 27, 2000, and had a magnitude of 4.3 (see Figure K.1). After reviewing data on injection volume, injection rate, downhole pressure, and percent of days injecting, the Bureau of Reclamation noted, "Of the four injection parameters investigated, the downhole pressure exhibits the best correlation with the occurrence of near-well seismicity over time" (Bureau of Reclamation, 2009). The Bureau of Reclamation also noted the record of seismic activity appears to be divided into three distinct clusters occurring from 1997 to January 2000, 2003 to 2005, and July 2008 to the present. The Bureau of Reclamation concludes, "There appears to be a gross correlation between the three periods of increased near-well seismic activity and periods of increased time-averaged injection pressures" (Bureau of Reclamation, 2010). These conclusions reiterate the results of other investigations into the cause of induced seismicity initiated by underground injection.

The Bureau of Reclamation continues to inject saline fluids underground as part of the Colorado River Basin Salinity Control Project, and it continues to control induced seismicity by the biennial shutdown of injection activity and by limiting the volume of fluid injected. Both of these actions minimize downhole injection pressure in an effort to limit induced seismic events.

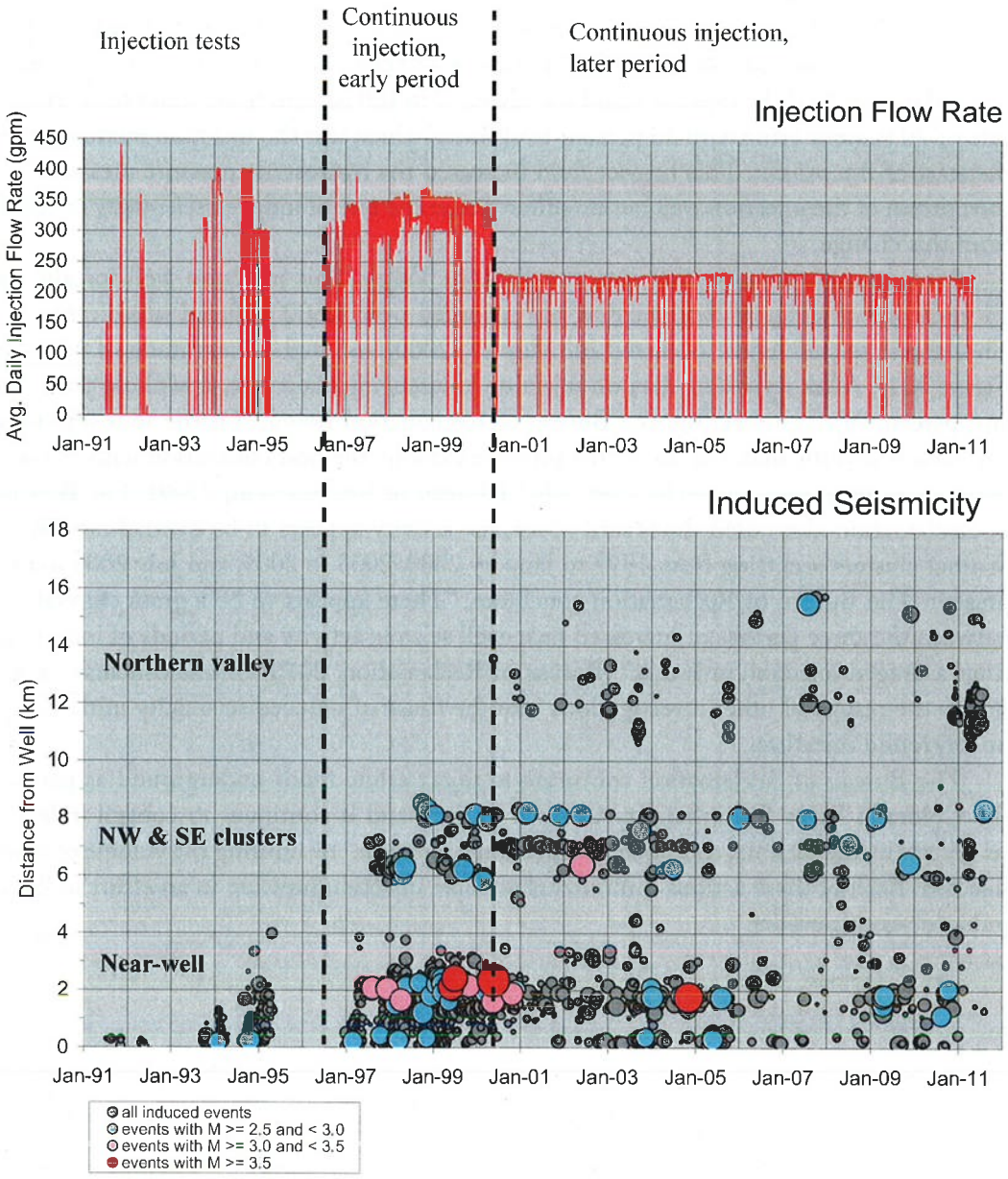

FIGURE K.1 Twenty-year data set collected by the Bureau of Reclamation for the Paradox Valley project. Upper figure shows the average daily injection flow rate in gallons per minute. Lower figure shows all induced events and their magnitudes over the same period with distance from the injection well. SOURCE: Block (2011).

APPENDIX K

REFERENCES

Block, L. 2011. Paradox Valley Deep Disposal Well and Induced Seismicity. Presentation to the National Research Council Committee on Induced Seismicity Potential in Energy Technologies, Dallas, TX, September 14.

Bureau of Reclamation. 2009. Overview of PVU-Induced Seismicity from 1996 to 2009 and implications for Future Injection Operations. Technical Memorandum No. 86-68330-2009-22.

Bureau of Reclamation. 2010. 2009 Annual Report Paradox Valley Seismic Network, Paradox Valley Project, Colorado. Technical Memorandum No. 86-68330-2010-07.

APPENDIX L

Estimated Injected Fluid Volumes

Tables L.1–L.5 contain the data used to create Figure 3.16.

TABLE L.1 Hydraulic Fracturing Volumes

Development Area	Average Volume Water (gal)	Volume Water Use Per Well (gal)	Volume Water Use Per Well (m^3)
Barnett	4,600,000	2,800,224	10,600
Eagle Ford	5,000,000	4,253,170	16,100
Haynesville	5,000,000	5,679,699	21,500
Marcellus	5,600,000	No data	No data
Niobrara	3,000,000	No data	No data
Average volume per well per day	4,640,000	—	—

NOTE: "Daily" hydraulic fracture volume plotted assumes the hydraulic fracturing procedure would take 2 days to complete; the 1-day volume plotted is half the total well volume estimated by King (2012). "Yearly" hydraulic fracture volume assumes 15 wells per year in the development area. Postfracturing flowback volume is assumed to be 20 percent of the total volume injected.
SOURCE: King (2012); Nicot and Scanlon (2012).

APPENDIX L

TABLE L.2 Carbon Capture and Sequestration Volumes

43 lb/ft^3	Density of liquid CO_2 at 80°C (AIRCO value)
2000 lb	1 ton liquid CO_2
47 ft^3	1 ton liquid CO_2 at 80°C
47,000,000 ft^3	1 million tons liquid CO_2 at 80°C per year
1,330,892 m^3	1 million tons liquid CO_2 at 80°C per year
351,355,488 gal	1 million tons liquid CO_2 at 80°C per year

Result:
1.33×10^6 m^3/year liquid CO_2 at 80°C per year
3.65×10^3 m^3/day liquid CO_2 at 80°C per year
3.51×10^8 gal/year liquid CO_2 at 80°C per year
9.63×10^5 gal/day liquid CO_2 at 80°C per year

NOTE: Table assumes 1 million tons of liquid CO_2 injection per year. The density/unit weight of liquid CO_2 varies significantly with temperature; the density of supercritical (liquid) CO_2 ranges from 0.60 to 0.75 g/cm^3 (Sminchak and Gupta, 2003). If one assumes approximately 43 lb/ft^3 (AIGA, 2009) for the unit weight of CO_2 (approximately 0.64 g/cm^3) at a subsurface temperature of 80°C (AIGA, 2009) then 1 ton of CO_2 equates to 47 ft^3, and 1 million tons/year equates to 47,000,000 ft^3/year or 1,330,892 m^3/year or 3646 m^3/day.
SOURCE: Sminchak and Gupta (2003); AIGA (2009).

TABLE L.3 Water Disposal Well Volume Calculations

9,000	bbl/day
42	gal/barrel
378,000	gal/day
137,970,000	gal/year

NOTE: Reported average saltwater disposal (SWD) injection of 8,000–11,000 bbl/day. SWD injection volumes estimated from Texas Railroad Commission for SWD wells north of DFW airport. Frohlich et al. (2010) report a survey of SWD wells in Tarrant and Johnson counties that reported rates ranging from 100,000 to 500,000 barrels per month; 9,000 bbl/day was used for graph. Nicot and Scanlon (2012) state Texas is the top shale producer in the United States.
SOURCE: Frohlich et al. (2010).

TABLE L.4 Geysers Geothermal Field Calculations

1,000,000,000	billion pounds steam/year
8	pounds steam/gallon
328,899	gal/day
120,048,019	gal/year

SOURCE: Smith et al. (2000).

TABLE L.5 Enhanced Geothermal Systems (EGS) Main Stimulation Calculations

11,500	m^3 water injected over 6 days
3,037,979	gallons water injected over 6 days
1,917	avg. m^3/day
506,330	avg. gal/day

SOURCE: Asanuma et al. (2008).

REFERENCES

AIGA (Asia Industrial Gases Association). 2009. *Carbon Dioxide*, 7th ed. Singapore: AIGA 068/10. Available at www.asiaiga.org/docs/AIGA%20068_10%20Carbon%20Dioxide_reformated%20Jan%2012.pdf (accessed May 2012).

Asanuma, H., Y. Kumano, H. Niitsuma, U. Schanz, and M. Häring. 2008. Interpretation of reservoir structure from super-resolution mapping of microseismic multiplets from stimulation at Basel, Switzerland in 2006. *GRC Transactions* 32:65-70.

Frohlich, C., C. Hayward, B. Stump, and E. Potter. 2010. The Dallas-Fort Worth earthquake sequence: October 2008-May 2009. *Bulletin of the Seismological Society of America* 101(1):327-340.

King, G.E. 2012. Hydraulic Fracturing 101: What every representative, environmentalist, regulator, reporter, investor, university researcher, neighbor, and engineer should know about estimating frac risk and improving frac performance in unconventional gas and oil wells. Paper SPE 152596 presented to the Society of Petroleum Engineers (SPE) Hydraulic Fracturing Technology Conference, The Woodlands, TX, February 6-8.

Nicot, J.-P., and B.R. Scanlon. 2012. Water use for shale-gas production in Texas, U.S. *Environmental Science and Technology* 46:3580-3586.

Sminchak, J., and N. Gupta. 2003. Aspects of induced seismic activity and deep-well sequestration of carbon dioxide. *Environmental Geosciences* 10(2):81-89.

Smith, J.L.B., J.J. Beall, and M.A. Stark. 2000. Induced seismicity in the SE Geysers Field, California, USA. Presented at the World Geothermal Congress, Kyushu-Tohoku, Japan, May 28-June 10.

APPENDIX M

Additional Acknowledgments

The committee gratefully acknowledges the support of three standing committees under the Board on Earth Sciences and Resources: the Committee on Earth Resources, the Committee on Geological and Geotechnical Engineering, and the Committee on Seismology and Geodynamics. In particular, the committee would like to thank the following people:

Committee on Earth Resources

Clayton R. Nichols, *Chair*
James A. Brierley
Elaine T. Cullen
Gonzalo Enciso
Michelle Michot Foss
Donald Juckett
Ann S. Maest
Leland L. "Roy" Mink
Mary M. Poulton
Arthur W. Ray
Norman H. Sleep
Richard J. Sweigard

Committee on Geological and Geotechnical Engineering

Edward Kavazanjian, Jr., *Chair*
John T. Christian
Patricia Culligan
Conrad W. Felice
Deborah J. Goodings
Murray W. Hitzman
James R. Rice
J. Carlos Santamarina

Committee on Seismology and Geodynamics

David T. Sandwell, *Chair*
Michael E. Wysession, *Vice-Chair*

APPENDIX M

J. Ramon Arrowsmith
Emily E. Brodsky
James L. Davis
Stuart Nishenko
Peter Olson
Nancy L. Ross
Charlotte A. Rowe
Brian W. Stump
Aaron A. Velasco